ISSN 1063-7842, Technical Physics, 2020, Vol. 65, No. 10, pp. 1622–1629. © Pleiades Publishing, Ltd., 2020.
Russian Text © The Author(s), 2020, published in Zhurnal Tekhnicheskoi Fiziki, 2020, Vol. 90, No. 10, pp. 1694–1701.

SOLID STATE

Studying High-Frequency Acoustic Emission during Discontinuous Creep in an Aluminum–Magnesium Alloy

A. A. Shibkov[a],*, M. A. Zheltov[a], M. F. Gasanov[a], A. E. Zolotov[a], A. A. Denisov[a], and S. S. Kochegarov[a]

[a] *Tambov State University, Tambov, 392000 Russia*

**e-mail: shibkov@tsu.tmb.ru*

Received February 21, 2020; revised March 17, 2020; accepted March 18, 2020

Abstract—Formation of macrolocalized deformation bands under conditions of serrated creep is studied by methods of acoustic emission (AE) and high-speed video recording. It is established that the fastest stages of the deformation band formation, which are related to the emergence of a band on the surface with subsequent accelerated expansion, are accompanied by generating a burst of an AE signal in the band of ~0.05–1 MHz. Hidden correlations in the complex structure of the acoustic burst were studied by methods of statistical and fractal analysis. The relation between the acoustic burst envelope and variation rate of the force response caused by the formation of an individual deformation band is established.

DOI: 10.1134/S1063784220100199

INTRODUCTION

It is well known that acoustic emission (AE) in deformed crystalline materials is generated by sharp relaxation of internal stresses, which is related to the dynamics of dislocation ensembles (slip lines and bands), twins, cracks, etc., reflecting the so-called "mesoscopic structure level" of plastic deformation of crystals [1–3]. In spite of intense analytical studies that have carried out of mechanisms of AE signal generation at this level [4–7], a convincing experimental proof of the dislocation nature of AE was obtained by filming the twin growth in a calcite crystal with simultaneous record of an acoustic signal [8]. Studying plastic instabilities by the AE method at the macroscopic level was carried out mainly under the conditions of the Portevin–Le Chatelier (PLC) effect—i.e., the appearance of repeating stress jumps under deformation with a given rate $\dot{\varepsilon}_0$ = const or deformation jumps under loading with a constant rate $\dot{\sigma}_0$ = const [9–18]. It is found that every jump of stress or deformation is accompanied by a discrete AE burst [10] which, according to visual observations, correlates with the formation of PLC deformation bands. In [11, 12], the AE method was combined with laser extensometry of the surface of deformed alloys of the Al–Mg system. The last, however, has an insufficient spatial resolution (~1–2 mm) and response time (~20 ms) for studying features of the dynamics of PLC deformation bands of different types A, B, and C. At the same time, present-day digital video cameras permit one to record propagating localized deformation bands with a resolution of ~10 μm/pixel and speed of up to several ten thousand frames per second [19–23], which allows one to record the early, fastest stage of the band formation, namely, the growth of the band nucleus—the incomplete band which intersects the sample cross section during the time of about 1 ms.

In our previous works [22, 23], the dynamics of deformation bands was studied by the AE method in the low-frequency region of ~10 Hz–10 kHz and, synchronously, by video recording of the surface with a time resolution of 40–50 μs under conditions of serrated creep of the AlMg6 aluminum–magnesium alloy. It is established that the main contribution to the acoustic signal is made by the formation of the completed band, which corroborates the mechanism of AE generation by dislocations emerging on the sample surface and the first peak in the AE burst with the growth time of ~1 ms well correlates with the jump of the stress drop rate. The aim of this work is to study the information carried by a high-frequency (in the band of ~0.05–1 MHz) discrete AE around the dynamics of an individual deformation band.

1. TECHNIQUE

We studied a polycrystalline AlMg6 aluminum–magnesium alloy. The alloy composition, thermal treatment, and technique of measuring jumps of deformation and load under conditions of serrated creep were expounded in [22–25]. The specificity of this work is using a Zetlab BC 601 high-frequency AE sensor with an almost plane amplitude–frequency characteristic (AFC) in a frequency range of ~100–800 kHz and a smooth decrease in the region of lower frequencies of <100 kHz. The AE signals were amplified by 40 dB with an AEP5 preamplifier (Vallen Sys-

teme) and continuously recorded without a threshold with an amplitude resolution of 16 bit and recorded frequency of 5 MHz. The low-frequency spectrum range studied earlier in [22, 23] was suppressed by a low-frequency filter (up to 50 kHz). The video recording rate with a Fastcam Mini UX 500/100 digital camera (Photron) was 5000 fps. To enhance the image contrast, as earlier, the technique of subtractions of time-consecutive digital images was used [24].

2. RESULTS AND DISCUSSION

2.1. Correlation of the AE Signal Envelope with the Kinetics of the Deformation Band Growth and Force Response

Samples of the AlMg6 alloy in the form of two-sided blades with the working part dimensions of 6 × 3 × 0.25 mm were loaded in two stages. First, this was done at a constant rate of the applied stress $\dot{\sigma}_0$ = 0.1 MPa/s to a fixed creep stress σ_0 = const (270–310 MPa) considerably exceeding the conventional yield strength $\sigma_{0.2}$ = 160 MPa. After some time (incubation time) depending on the creep stress, a localized plastic deformation band is spontaneously generated and grows on the sample surface; the band is a trigger for the development of the deformation step with an amplitude of ~1–5% on the creep curve. The band is usually generated in a random position on the surface of the working part of the sample or near one of the blades. Such a case is presented in Fig. 1, which shows a fragment of the record of generation and growth of the incomplete arc-shaped band.

The results of image processing in the form of the kinetic curve of the length growth L_b, speed of the vertex v_t, band area S, and band growth rate $\overline{S}$, as well as acoustic signal $\varphi_{AE}(t)$, are presented in Fig. 2. The time dependences of geometric parameters of an incomplete band exhibit a typical nonlinear dynamics with an abrupt acceleration at the final stage of the growth. Note that, due to the decrease in the stress level in the region of the blade, the growth rate of the incomplete arc-shaped band is somewhat less than the growth rate of the band in the central region of the working part where the band grows in the direction of maximum tangential stresses. The direction makes an angle of 58°–60° with the axis of tension [19–24]. The time of emergence of the band on the opposite lateral surface coincides with the peaks of the AE signal, tip velocity v_t, and growth rate of the band area $\overline{S}$. In [22, 23], the signal of low-frequency discrete AE in the band of 10 Hz–10 kHz was obtained and studied; in contrast to that signal, the high-frequency signal has a more complicated structure in a wide frequency band (Fig. 3) from the lower 50-kHz frequency related to filtration of low frequencies to ~1 MHz, which is caused mainly by the upper AFC frequency of the used sensor.

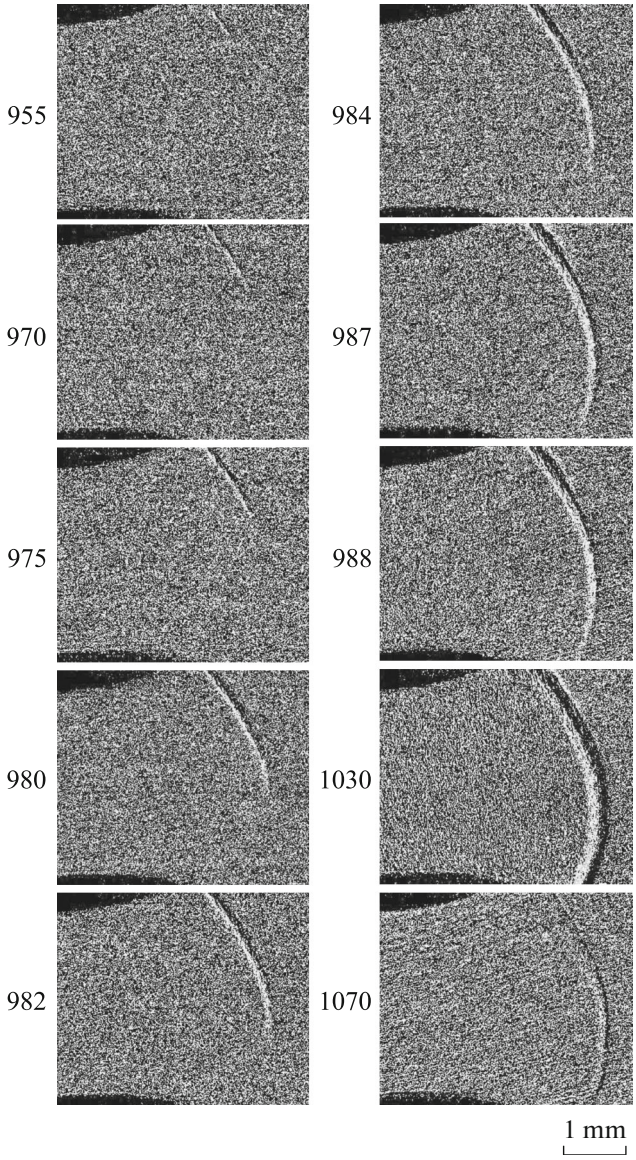

Fig. 1. Formation of the primary deformation band which is a trigger for the development of the deformation jump in the AlMg6 alloy under conditions of serrated creep at $\sigma_0 \approx$ 285 MPa. The shooting speed is 5000 fps. The numerals indicate the numbers of video recording frames.

Thus, formation of the deformation band is accompanied by a broadband acoustic burst, power spectrum $P(f)$ of which contains in fact all frequencies of the range under study with the main peak near 100 kHz (Fig. 3) and median frequency $f_m \approx$ 300 kHz determined, according to [26], from the condition

$$\int_0^{f_m} P(f)df = \int_{f_m}^{\infty} P(f)df,$$

and the envelope of the AE signal is bell-shaped with a maximum at the time of the formation of the complete band (Fig. 2).

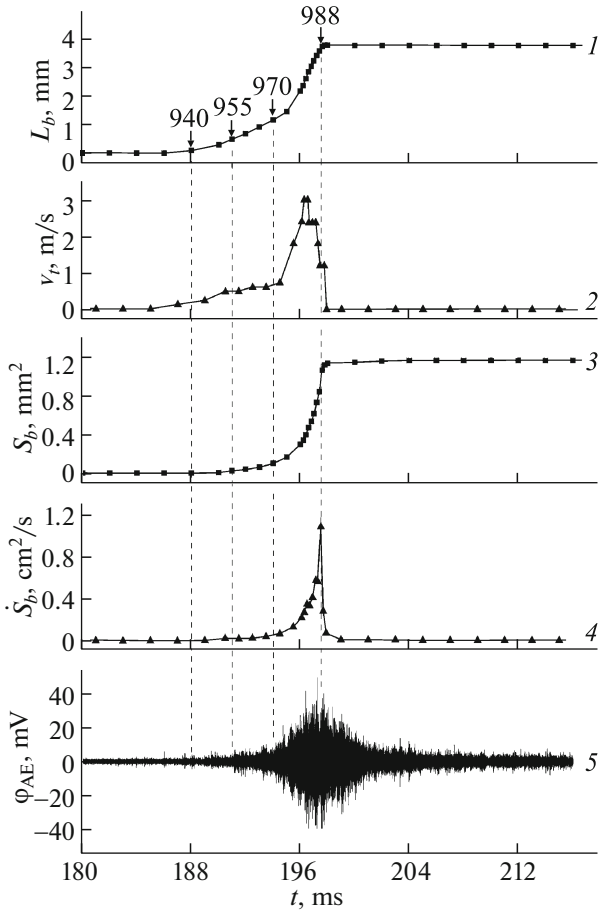

Fig. 2. Time dependences of different characteristics of the primary deformation band: (*1*) band length $L_b(t)$, (*2*) speed of tip velocity $v_t(t)$, (*3*) band area $S(t)$, (*4*) growth rate of band area $\dot{S}(t)$, and (*5*) AE signal φ_{AE}.

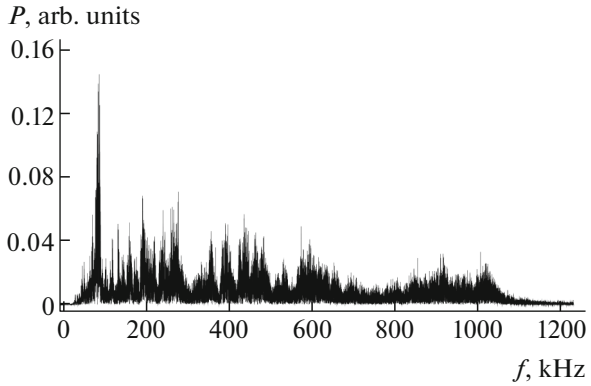

Fig. 3. Power spectrum $P(f)$ of the AE signal presented in Fig. 2, curve *5*.

It follows from Fig. 2 that the main contribution to the acoustic burst is made by the stage of accelerated growth of the incomplete band before its emergence on the opposite surface of the sample, i.e., the time of the formation of the complete band. This stage corresponds approximately to the second half of the band length growth (frames 970–988 in Fig. 1). The preceding stage with the tip velocity $v_t < 0.5$ m/s, including the band generation time itself, yields a relatively weak AE signal not exceeding the level of the continuous component of the acoustic signal. The stage of the acoustic burst decay after the time of the formation of the complete band (frame 988 in Fig. 1) approximately coincides with the stage at which the growth rate of the band area $\dot{S}_b(t)$ decays; the duration of the latter is ~1 ms. The corresponding stage of the acoustic burst is apparently characterized by the dynamics of dislocation avalanches inside the band and, probably, effects of acoustic wave reflection from the sample surface. The latter, however, are possible only at frequencies $f > 1$ MHz, when the length of the acoustic wave λ turns out to be comparable with the sample size d or less than it: $\lambda = c/f_{max} \approx 5$ mm, where $c \approx 5 \times 10^3$ m/s is the speed of sound. As seen from Fig. 3, this spectrum region ("the high-frequency tail") constitutes only a small part (<10%) of the power spectrum. For this reason, possible effects of acoustic wave reflection at frequencies of ~1 MHz cannot explain the complex broadband structure of the AE burst generated during the formation of the deformation band.

Since the typical duration of a high-frequency AE signal burst is ~3–10 ms, i.e., is commensurable with the duration of the stress drop front, it is interesting to study the correlation of the averaged AE burst envelope with the force response (more exactly, with the shape of function $\psi(t) = |d\sigma(t)/dt|$). Figure 4 presents the force and acoustic responses to the formation of an individual deformation band in the form of unload jump $\sigma(t)$ and acoustic burst $\varphi_{AE}(t)$ for comparison with the shape of function $\psi(t)$. The averaged envelope of the acoustic burst was calculated in the form

$$\xi(t) = \langle|\varphi_{AE}(t)|\rangle = \Delta t^{-1}\int_{t}^{t+\Delta t}|\varphi_{AE}(t')|dt', \qquad (1)$$

where Δt and $|\varphi_{AE}(t)|$ are the averaging time and absolute value of the AE signal, respectively. Since the load was recorded at a rate of 2 kHz, the averaging time was chosen to be $\Delta t = 0.5$ ms. Bell-shaped time dependences $\xi(t)$ and $\psi(\xi)$ averaged at the same time Δt (=0.5 ms) are presented in Fig. 4 (curves *4*, *5*, respectively). According to calculations using the Mathcad software package, coefficient of correlation between these dependences $k \approx 0.9316$.

Another indicator of the correlation between functions $\xi(t)$ and $\psi(\xi)$ is the approximately linear dependence between their amplitudes $\Delta\xi_m$ and $\Delta\psi_m$ (Fig. 5). Therefore, the averaged envelope of the high-frequency acoustic signal modulus carries information about the variation rate of the force response $|\dot{\sigma}|$. This result coincides with conclusions of [23] devoted to correlations between the function $\psi(t)$ and amplitude

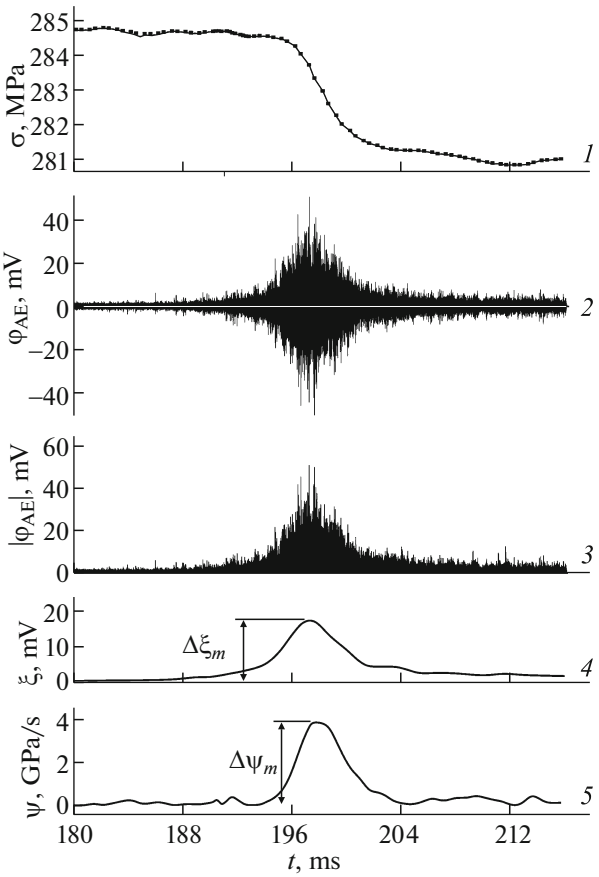

Fig. 4. (*1*) Jump of unloading σ and (*2*) acoustic burst φ_{AE} caused by the formation of an individual deformation band, (*3*) absolute value of the AE signal $|\varphi_{AE}|$, (*4*) its envelope ξ, and (*5*) absolute stress variation rate $\phi = |\dot{\sigma}|$. $\Delta\xi_m$ and $\Delta\psi_m$ are the amplitudes of the envelope of the acoustic burst and jump of the stress variation rate, respectively.

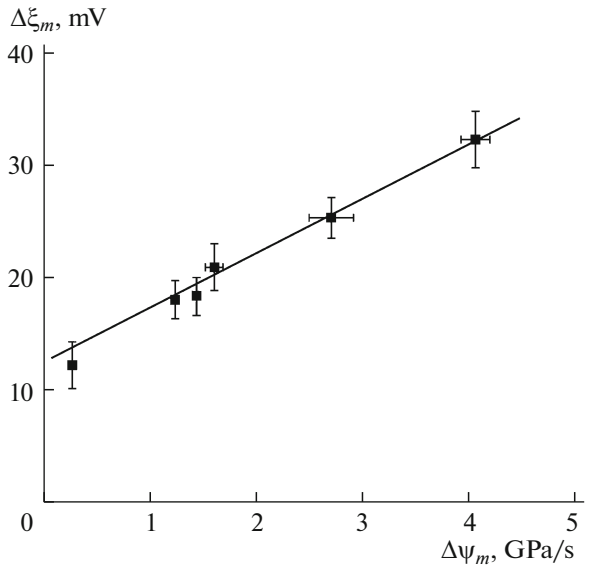

Fig. 5. Amplitude of the envelope $\Delta\xi_m$ of an AE burst caused by the formation of the individual deformation band as a function of the amplitude of the variation rate of the force response $\Delta\psi_m$.

of a low-frequency (in the band of 10 Hz–10 kHz) AE signal caused by the formation of individual deformation bands.

It is seen from Fig. 5 that the acoustic burst accompanying the formation of an individual deformation band has a complex fractal-like structure consisting of a large number of short (with a duration of ~1–10 μs) discrete pulses with different amplitudes. It is natural to hypothesize that these AE pulses are related to the dynamics of different-scale dislocation avalanches taking part in the evolution of the complex spatiotemporal structure of the macrolocalized deformation band. Therefore, it is of interest to study the temporal structure of the acoustic burst by methods of statistical, correlation, and fractal analysis.

2.2. Statistical and Fractal Analysis of the Acoustic Response Structure

First, the lower threshold of the signal amplitude in the structure of the acoustic burst twice exceeding the root-mean-square value of the AE signal several seconds before the time of generation of the primary deformation band was established (approximately in the middle of the plateau between steps on the creep curve). Then, total number N of AE pulses above this threshold was counted (in the example presented in Fig. 6, $N = 2643$) and statistical distribution function $D(s) = N^{-1}dN/ds$ of the normalized energy of acoustic pulses $s = A^2/\overline{A}^2$ was constructed. Here, $A = \varphi_m$ is the amplitude of the AE pulse, A^2 (= E) is the energy characteristic of an individual AE pulse in the AE burst structure, $\overline{A}^2$ is the average value of the squared amplitude of AE signals, and dN is the number of AE pulses the amplitude of which falls within the narrow interval $(s - \delta s/2, s + \delta s/2)$.

The statistical distribution function of squared amplitudes $D(s)$ presented in Fig. 7 has a hyperbolic shape, i.e., differs greatly from the normal distribution peculiar to a random process. In double logarithmic coordinates, the dependence of log$D$ on log$s$ is approximately linear with a slope to the s-axis equal to −2.23. This means that amplitude distribution $D(s)$ obeys the power law

$$D(s) \sim s^{-\alpha} \qquad (2)$$

with exponent $\alpha = 2.23$. The power distribution of squared amplitudes of AE pulses indicates self-similarity of the acoustic signal, i.e., the absence of the distinguished scale of events (scale invariance) peculiar to fractal time series [27, 28].

The obtained result agrees with results of numerical simulation of self-organizing dislocation avalanches at the second and third creep stages [29], as well as with

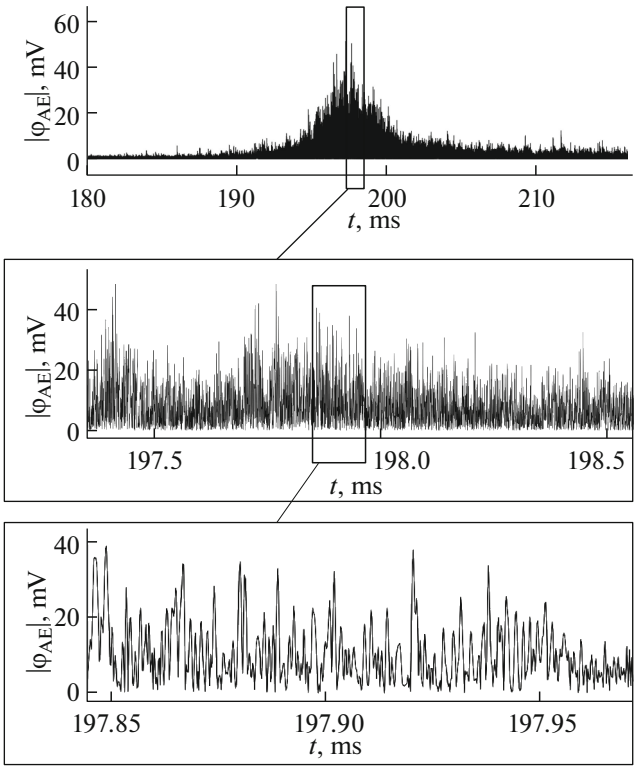

Fig. 6. Temporal structure at different time scales of an AE burst caused by the formation of an individual deformation band in the AlMg6 alloy.

data of AE signal measurement of during the creep deformation of single crystals of ice [30, 31] and acoustic bursts under conditions of the PLC effect manifestation in metals [32–35]. Numerical investigation on ice single crystals characterized by slip in the basal plane demonstrates the formation of dislocation dipoles and walls during the creep. They form the structure of holding forces, which leads to the formation of dislocation avalanches of different scales, and the amplitude distribution of AE signals is demonstrated by a power law [29]. For pure single crystals of ice, Cu, Zn, and Cd, power exponent $\alpha \approx 1.8$–2.15 [36, 37]. Experimental studies of the discrete AE under conditions of the PLC effect on polycrystalline Al–Mg alloys with a magnesium content of 3–6% yield α within the interval from 2 to 3 [32–35]. Large values of α are caused, as believed in [32], by multiple slip, presence of precipitates, grain boundaries, forest dislocations, and impurity atoms as effective obstacles of the dislocation motion, which increases the fraction of small dislocation avalanches and decreases the fraction of large ones and, therefore, increases power exponent α.

Note that a classical example of self-organization of collective dynamic processes is earthquakes. The earthquake magnitude is usually measured in terms of energy E released during a slip of tectonic plates and the statistical distribution of magnitudes $D(E)$ follows the power law $D(E) \sim E^{-\alpha}$, where exponent α depends on earthquake geography and lies within the range from 1.8 to 2.2 [27].

Thus, spontaneous formation of deformation bands at a creep stress considerably exceeding the yield strength is similar to earthquakes and corresponding seismic signals in the threshold dynamics and statistical distribution of the energy of acoustic signals in the structure of the AE burst. They are characterized by slow accumulation of internal stresses with subsequent

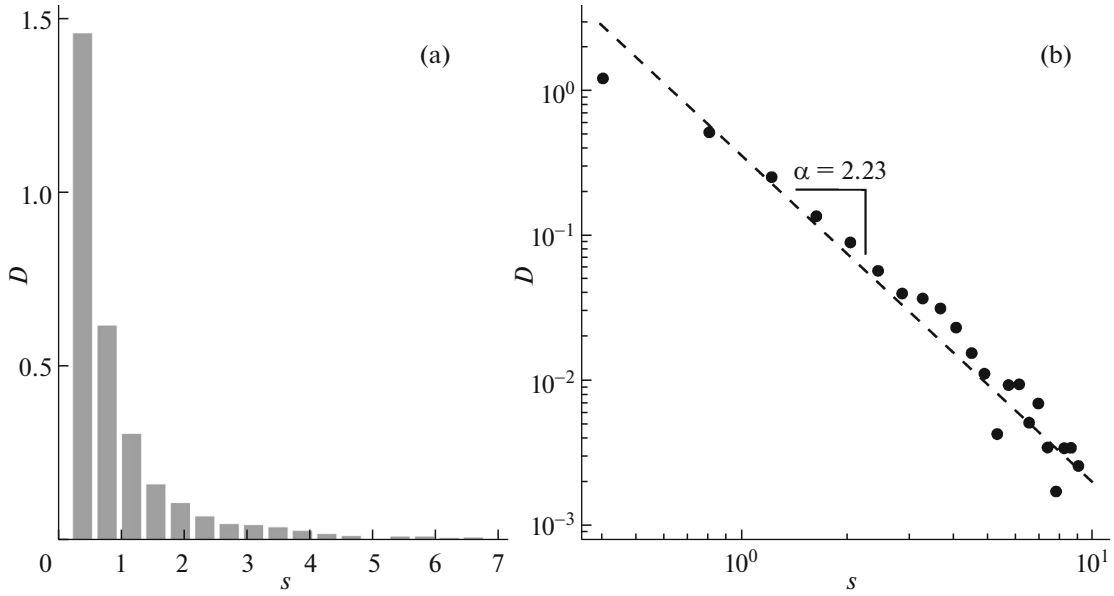

Fig. 7. Amplitude distribution of discrete AE signals in the structure of an acoustic burst caused by the formation of an individual deformation band: (a) in the D–s coordinates and (b) in double logarithmic coordinates.

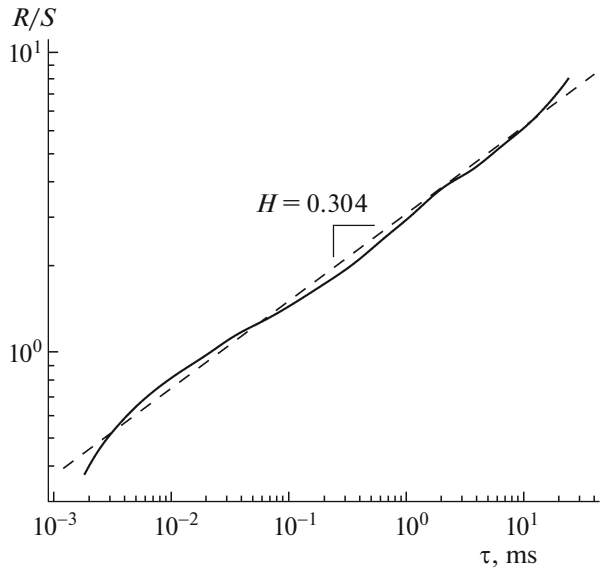

Fig. 8. Results of Hurst R/S analysis: dependence of the normalized R/S range on τ in double logarithmic coordinates; the slope of the dashed line yields the Hurst exponent $H = 0.304$.

spontaneous rapid relaxation in the form of collective self-organizing avalanches. This is indicated by the power law of the amplitude distribution of AE signals, which is one of the attributes of long-range correlations covering the whole system or a considerable part of it.

Another attribute of self-similarity and presence of hidden correlations of an acoustic signal is its monofractality. The fractal dimension of the signal was calculated using the Hurst R/S-analysis by the normalized range method [28] be means of the expression

$$R/S \sim \tau^H, \tag{3}$$

where $R(\tau) = Y_{\max} - Y_{\min}$ is the accumulated deviation (range) of signal $\varphi_{AE}(t)$ from the mean value on time interval τ and the accumulated deviation is determined as

$$Y(t,\tau) = \int_0^t [\varphi_{AE}(t') - \langle\varphi_{AE}\rangle_\tau]dt', \tag{4}$$

where

$$\langle\varphi_{AE}\rangle_\tau = \tau^{-1}\int_0^\tau \varphi_{AE}(t)dt$$

and

$$S(\tau) = \left\{\tau^{-1}\int_0^\tau [\varphi_{AE}(t) - \langle\varphi_{AE}\rangle_\tau]^2 dt'\right\}^{1/2}$$

are the mean value and standard deviation of time series $\varphi_{AE}(t)$ on interval τ, H is the Hurst exponent, and the fractal dimension of the time series is determined as $D_f = 2 - H$ [28].

Figure 8 shows the dependence of quantity R/S on time interval τ in double logarithmic coordinates. The linear approximation of this dependence yields the Hurst exponent $H = 0.304$. It is seen that the acoustic burst caused by the formation of an individual deformation band is of monofractal nature with dimension $D_f = 1.696$ and scaling of about one-and-a-half orders in the normalized range R/S. Note that, for white noise (noncorrelated process), $H = 0.5$, while the value $H = 0.5$ indicates signal antipersistence. This means that, if the signal amplitude increases on a certain time interval, one should expect that it will decrease on the next time interval with approximately the same duration; conversely, if the signal amplitude decreases on interval τ, then, as a result of internal correlation of the signal, its amplitude will increase on the next time interval with the same duration.

This property of the acoustic signal can reflect alternation of acoustic activity related to the dynamics of comparatively large dislocation avalanches in the structure of the deformation band and periods of its decay due to relaxation of internal stresses and, conversely, during the time of relatively low activity of the AE signal, the material accumulates internal stresses. Their subsequent relaxation produces a burst of acoustic activity, and so on.

CONCLUSIONS

The dynamics of the formation of macrolocalized deformation bands has been studied in situ using synchronous registering of data of the force response, high-speed video recording with a speed of 5000 fps, and acoustic response in the frequency band from ~50 kHz to ~1 MHz under conditions of serrated creep of the AlMg6 aluminum–magnesium alloy. It has been established that the earliest and fastest stage of the deformation band formation having a duration of several milliseconds and related to the generation and growth of the band nucleus, emergence on the surface, and subsequent fast expansion of the band, is accompanied by generation of an AE burst with a duration of ~3–10 ms.

The complex structure of this burst includes $\sim 10^3$ discrete AE pulses with a duration of ~1–10 μs and different amplitudes. The shape and amplitude of the acoustic burst envelope are the most informative characteristics of the AE burst caused by the formation of an individual deformation band. It is established that they well correlate with the shape and amplitude of the growth rate of the unload jump of the machine–sample system.

The power distribution functions of amplitudes of discrete AE signals in the acoustic burst structure during the formation of the band, as well as monofractality of the temporal structure of the AE burst with

fractal dimension $D_f \approx 1.7$ calculated using the Hurst R/S analysis, have been revealed. The obtained results testify to the collective self-organizing dynamics of dislocation avalanches in the structure of the forming macrolocalized deformation band.

The results obtained in [22, 23] and in this work give a direct experimental proof of the dislocation nature of AE signals accompanying the serrated deformation of metals and alloys. The proof is based on the established relation between the AE signal burst and the dynamics of deformation bands. In addition, in those works, the information content of the low-frequency (in the audio range) and high-frequency (ultrasonic) component of the acoustic signal generated during the formation of deformation bands in the aluminum–magnesium alloy was revealed.

FUNDING

The complex high-speed experimental in situ studies of the dynamics of deformation bands were supported in part by the Russian Science Foundation, project no. 18-19-00304. The statistical and fractal analysis of acoustic signals was supported by the Russian Foundation for Basic Research, project no. 19-08-00395.

CONFLICT OF INTEREST

The authors declare that they have no conflicts of interest.

REFERENCES

1. V. E. Panin, V. A. Likhachev, and Yu. V. Grinyaev, *Structural Deformation Levels of Solids* (Nauka, Novosibirsk, 1985) [in Russian].
2. D. R. James and S. H. Carpenter, J. Appl. Phys. **42** (12), 4685 (1971). https://doi.org/10.1063/1.1659840
3. K. Mathis and F. Chmelik, in *Acoustic Emission,* Ed. by W. Sikorski (InTech, Rijeka, 2012), pp. 23–48.
4. V. S. Boiko and V. D. Natsik, *Elementary Processes of Plastic Deformation of Crystals* (Naukova Dumka, Kiev, 1978), pp. 159–189 [in Russian].
5. V. D. Natsik and K. A. Chishko, Akust. Zh. **38** (3), 511 (1992).
6. D. Rouby, P. Fleischmann, and C. Duvergier, Philos. Mag. A **47** (5), 671 (1983).
7. D. Rouby, P. Fleischmann, and C. Duvergier, Philos. Mag. A **47** (5), 689 (1983).
8. B. C. Boiko, R. I. Garber, and V. F. Kivshik, Fiz. Tverd. Tela **17** (5), 1541 (1975).
9. W. F. Hartman, Exp. Mech. **14**, 19 (1974). https://doi.org/10.1007/BF02324855
10. M. M. Krishtal and D. L. Merson, Phys. Met. Metallogr. **81** (1), 104 (1996).
11. F. Chmelik, A. Ziegenbein, H. Neuhauser, and P. Lukac, Mater. Sci. Eng., A **324**, 200 (2002). https://doi.org/10.1016/S0921-5093(01)01312-0
12. F. Chmelik, F. B. Klose, H. Dierke, J. Sachl, H. Neuhauser, and P. Lukac, Mater. Sci. Eng., A **462**, 53 (2007). https://doi.org/10.1016/j.msea.2006.01.169
13. M. M. Krishtal, A. K. Khrustalev, A. A. Razuvaev, and I. S. Demin, Deform. Razrush. Mater., No. 1, 28 (2008).
14. M. A. Lebyodkin, T. A. Lebedkina, F. Chmelik, T. T. Lamark, Y. Estrin, C. Fressengeas, and J. Weiss, Phys. Rev. B **79**, 174114 (2009). https://doi.org/10.1103/PhysRevB.79.174114
15. M. A. Lebyodkin, N. P. Kobelev, Y. Bougherira, D. Entemeyer, C. Fressengeas, V. S. Gornakov, T. A. Lebedkina, and I. V. Shashkov, Acta Mater. **60**, 3729 (2012). https://doi.org/10.1016/j.actamat.2012.03.029
16. I. V. Shashkov, M. A. Lebyodkin, and T. A. Lebedkina, Acta Mater. **60**, 6842 (2012). https://doi.org/10.1016/j.actamat.2012.08.058
17. M. A. Lebyodkin, I. V. Shashkov, and T. A. Lebedkina, Phys. Rev. E **88**, 042402 (2013). https://doi.org/10.1103/PhysRevE.88.042402
18. J. Kumar, R. Sarmah, and G. Ananthakrishna, Phys. Rev. B **92**, 144109 (2015). https://doi.org/10.1103/PhysRevB.92.144109
19. M. M. Krishtal, A. K. Khrustalev, A. V. Volkov, and S. A. Borodin, Dokl. Phys. **54** (5), 225 (2009). https://doi.org/10.1134/S1028335809050024
20. W. Tong, H. Tao, N. Zhang, and L. G. Hector, Scripta Mater. **53**, 87 (2005). https://doi.org/10.1016/j.scriptamat.2005.03.020
21. G. F. Xiang, Q. C. Zhang, H. W. Liu, X. P. Wu, and X. Y. Ju, Scripta Mater. **56**, 721 (2007). https://doi.org/10.1016/j.scriptamat.2006.08.049
22. A. A. Shibkov, M. A. Zheltov, M. F. Gasanov, and A. E. Zolotov, Phys. Solid State **59** (12), 2387 (2017). https://doi.org/10.1134/S1063783417120289
23. A. A. Shibkov, M. A. Zheltov, M. F. Gasanov, A. E. Zolotov, A. A. Denisov, M. A. Lebyodkin, Mater. Sci. Eng., A **772**, 138777 (2020). https://doi.org/10.1016/j.msea.2019.138777
24. A. A. Shibkov, M. F. Gasanov, M. A. Zheltov, A. E. Zolotov, V. I. Ivolgin, Int. J. Plast. **86**, 37 (2016). https://doi.org/10.1016/j.ijplas.2016.07.014
25. A. A. Shibkov, A. A. Mazilkin, S. G. Ppotasova, D. V. Mikhlik, A. E. Zolotov, M. A. Zheltov, and A. V. Shuklinov, Deform. Razrush. Mater., No. 5, 24 (2008).
26. A. Vinogradov and A. Lasarev, Scripta Mater. **66**, 745 (2012). https://doi.org/10.1016/j.scriptamat.2012.01.053
27. H. J. Jensen, *Self-Organized Criticality* (Cambridge Univ. Press, Cambridge, 1998).
28. J. Feder, *Fractals* (Springer, New York, 1988).
29. M. C. Miguel, A. Vesplignanl, S. Zapperi, J. Weiss, and J.-R. Grasso, Nature **410** (4), 667 (2001). https://doi.org/10.1038/35070524
30. J. Weiss and J.-R. Grasso, J. Phys. Chem. B **101** (32), 6113 (1997). https://doi.org/10.1021/jp963157f

31. J. Weiss, J.-R. Grasso, M.-C. Miguel, A. Vespignani, and S. Zapperi, Mater. Sci. Eng., A **309–310**, 360 (2001). PII: S0921-5093(00)01633-6
32. M. A. Lebyodkin, N. P. Kobelev, Y. Bougherira, D. Entemeyer, C. Fressengeas, V. S. Gornakov, T. A. Lebedkina, and I. V. Shashkov, Acta Mater. **60**, 3729 (2012). https://doi.org/10.1016/j.actamat.2012.03.026
33. M. A. Lebyodkin, I. V. Shashkov, T. A. Lebedkina, K. Mathis, P. Dobron, and F. Chmelik, Phys. Rev. E **88**, 042402 (2013). https://doi.org/10.1103/PhysRevE.88.042402
34. T. A. Lebedkina, D. A. Zhemchuzhnikova, and M. A. Lebyodkin, Phys. Rev. E **97**, 013001 (2018). https://doi.org/10.1103/PhysRevE.97.013001
35. I. V. Shashkov, M. A. Lebyodkin, and T. A. Lebedkina, Acta Mater. **60**, 6842 (2012). https://doi.org/10.1016/j.actamat.2012.08.058
36. J. Weiss and F. Louchet, Scripta Mater. **54**, 747 (2006). https://doi.org/10.1016/j.scriptamat.2005.10.056
37. J. Weiss, T. Richeton, F. Louchet, F. Chmelik, P. Dodron, D. Entemeyer, M. Lebyodkin, T. Lebedkina, C. Fressengeas, and R. J. McDonald, Phys. Rev. B **76**, 224110 (2007). https://doi.org/10.1103/PhysRevB.76.224110

Translated by A. Nikol'skii